Wideband 45° linearly polarized slot array antenna based on gap waveguide technology for 5G millimeter-wave applications

Zhang, Ling; Lu, Yunlong; You, Yang; Zhu, Qi Ang; Wang, Yi; Yang, Wen Wen; Huang, Jifu

DOI:
10.1109/LAWP.2021.3077286

Wideband 45° Linearly Polarized Slot Array Antenna Based on Gap Waveguide Technology for 5G Millimeter-Wave Applications

Ling Zhang, Yunlong Lu, Yang You, Qi-Ang Zhu, Yi Wang, *Senior Member, IEEE*, Wen-Wen Yang, *Member, IEEE,* and Jifu Huang

***Abstract*— This letter presents a wideband high performance 45° linearly polarization 8×8-slot array antenna. The gap waveguide technology is utilized to realize the proposed antenna, so that the electromagnetic (EM) leakage among the metallic blocks can be cancelled. 2×4-slot sub-arrays are used to construct the array antenna. An additional cavity power divider layer is inserted between the layers of original cavity power dividers and radiation slots to balance the amplitude and phase distributions in wideband frequency band. This suppresses the grating lobes. Triangular blocks are loaded in the new cavity power divider layer to confine the EM field distribution, thereby improving cross polarization discrimination (XPD). For demonstration, a prototype antenna covering 5G mmW NR bands of 257, 258 and 261 is design, fabricated and measured. Measured results show that an impedance bandwidth of 23-30 GHz (|S_{11}|<-10.5 dB) is achieved. Within this frequency band, the peak gain and antenna efficiency are more than 24.6 dBi and 76.3%. In addition, the sidelobe level (SLL) of lower than -25.8 dB and XPD of better than 30.2 dB are also obtained over the same frequency band.**

Keywords— *Slot arrays, gap waveguide, millimeter wave antennas, low SLLs, high cross polarization discrimination.*

I. Introduction

The frequency bands of n257 (26.5 - 29.5 GHz), n258 (24.25 - 27.5 GHz), and n261 (27.5 - 28.35 GHz) have been allocated to the 5G millimeter-wave (mmW) communication applications, which support high-data rate transmission [1]-[3]. Antennas with wideband, high-gain and low sidelobe levels (SLLs) are essential to achieve the performance goal over a long distance [4]. Corporate-fed slot array antenna based on hollow-waveguide is a popular choice [5]-[11] due to its low-loss and high-efficiency capability. To achieve low SLLs, amplitude tapering and 45° linearly polarized technologies are two effective methods for high-gain slot array antennas [6]. One advantage of the 45° technology over the amplitude tapering is that it does not sacrifice antenna efficiency [8]-[10]. However, one major challenge for hollow-waveguide based antennas arises with their multi-layer configuration. The quality of the electrical contact between the metallic layers has a major impact on the performance [12].

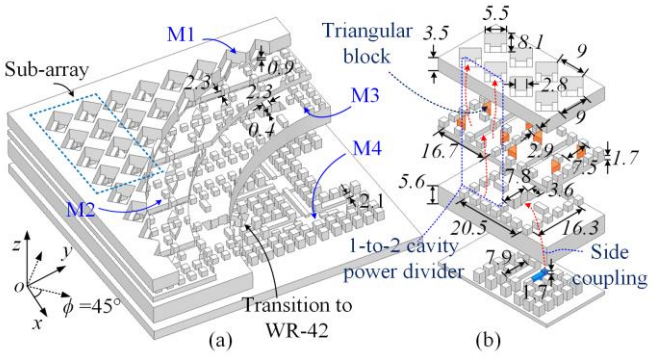

Fig. 1. Configuration of the proposed array antenna. (a) 3-D overview; (b) Sub-array. Definition of principal and intended E- and H-planes are: ϕ = 0° (principal E-plane), ϕ = 90°(principal H-plane) , ϕ = 45°(intended E-plane) and ϕ = 135°(intended H-plane). All dimensions are given in millimeters.

The gap waveguide (GW), as a relatively new guiding structure for mmW, could overcome some of these limitations of metallic waveguide [13]-[16]. Over the past few years, some slot array antennas based on different types of GWs were investigated [17]-[19]. To further reduce the complexity, antennas only with two metallic layers have also been developed [18], [19]. But, the fractional bandwidth (FBW) was limited to 17% and low SLL was not considered. In [20], a V-band slot array antenna based on ridge GW was reported. 10°-tilted radiation slots were used to improve the radiation pattern envelops without sacrificing aperture efficiency. Similarly, only 17.6% of FBW was achieved, and the cross-polarization level deteriorates when SLL is further improved using a larger titling angle.

This letter presents a wideband 8 × 8-slot array antenna with ridge GW-based corporate-fed network. An additional 1-to-2 cavity power divider layer is inserted between the 45°-tilted radiation slot layer and the original 1-to-4 cavity power divider to optimize the amplitude and phase distributions of the excitation signals among the radiation slots. This leads to the replacement of conventional 2×2-slot array element with a 2×4-slot sub-array. In order to improve the cross-polarization

This work was supported partly by National Key R&D Program of China under Project 2018YFB1802100, in part by National Natural Science Foundation of China under Projects 61801252, U1809203 and 61631012, in part by Zhejiang Natural Science Foundation under Project LY21F010002, Guangdong R&D Project in Key Areas under grant no. 2019B010156004, Ningbo Natural Science Foundation under Project 202003N4108 and the Fundamental Research Funds for the Provincial Universities of Zhejiang under grant no. SJLY2020001. (*Corresponding author: Yunlong Lu; Jifu Huang.*)

L. Zhang, Y. Lu, Y. You, Q. Zhu, and J. Huang are with the Faculty of Electrical Engineering and Computer Science, Ningbo University, Ningbo, Zhejiang, 315211, China (e-mail: luyunlong@nbu.edu.cn).

Y. Wang is with School of Engineering, University of Birmingham, B15 2TT, United Kingdom (e-mail: y.wang.1@bham.ac.uk).

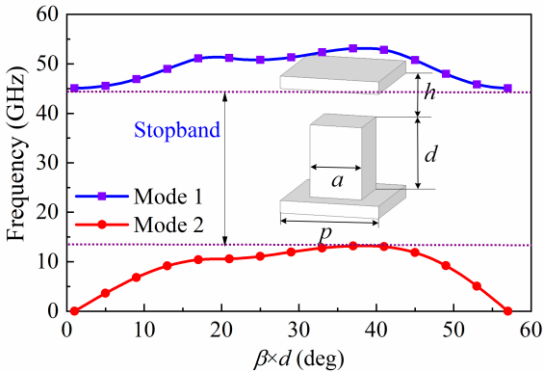

Fig. 2. Dispersion diagram of a pin unit cell with periodic boundary.

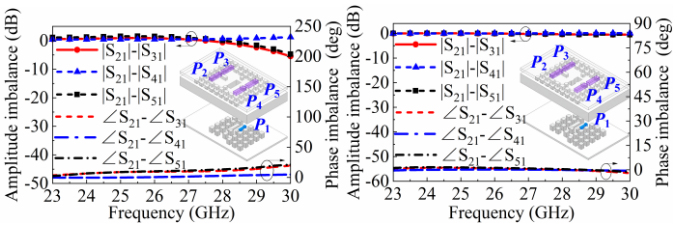

Fig. 3. Simulated amplitude and phase response based on (a) hollow waveguide coupling and (b) double-ridge waveguide coupling.

discrimination (XPD) over a wide frequency band, triangular blocks are loaded at the cavity corners in the cavity power divider layer to confine E-field along the E-plane. The demonstrate antenna exhibits high performances of wideband, low SLLs, high efficiency and XPD.

II. Antenna Configuration

The configurations of the whole array antenna and the sub-array are shown in Fig. 1(a) and (b). It is a 8×8-slot 45° linearly polarized array antenna, formed of the radiation part and the feed network part. The radiation part consists of three metallic layers: radiation-slot layer (M1) and cavity power divider layers (M2 and M3). The feed network in M4 is a power divider with equal amplitude and in-phase response. A 2×4-slot sub-array is used to build the whole antenna. One 1-to-4 cavity power divider (M3), cascaded with four 1-to-2 cavity power dividers (M2), in each sub-array form the 1-to-8 (2×4) vertical power divider. The signals from the feed network enter into the 1-to-8 (2×4) dividers and excite the radiation slots. The coordinate system, as well as the definition of intended and principal E- and H-planes, is shown in Fig. 1(a). The frequency band of 23–30 GHz is chosen to support 5G mmW communication. Except the radiation-slot layer (M1), others (M2-M4) are realized based on gap waveguide. Design detail of each part is introduced in the following sections.

III. Antenna Analysis and Design

A. Dispersion diagram of GW

The array antenna is based on GW technology. The periodic pins in the feed network (M4) and cavity power divider layers (M2 and M3) present a stopband for parallel-plate modes, which prevents the electromagnetic (EM) leakage between the metallic layers. The pin size is suitably designed to control the operating frequency band of array antenna within the stopband.

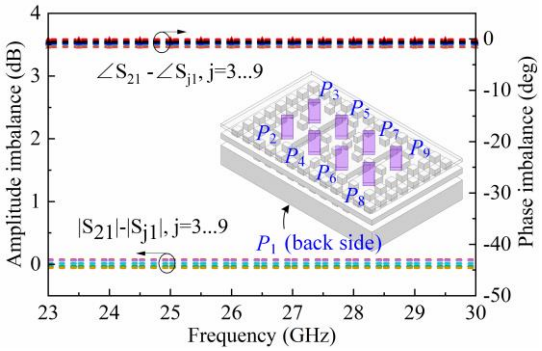

Fig. 4. Simulated S-parameters of the combined 1-to-8 vertical power divider.

Thus, the EM leakage in the antenna operating frequency band can be prevented.

Fig. 2 shows the calculated dispersion diagram of GW based on a pin unit cell with periodic boundary condition. The pin dimensions are: p = 4 mm, a = 2.1 mm, h = 0.1 mm and d = 2.9 mm. It can be seen that the stopband is from 13 GHz to 45 GHz, which covers the concerned operation frequency band of the antenna.

B. Sub-array

The sub-array consists of 2×4 cavity-backed slots, as shown in Fig. 1(b). The adjacent slots in M1 have a space of close to but less than one wavelength (free space wavelength corresponding to the highest frequency in the operating band) to avoid the grating lobes. The flared radiation slots are utilized to reduce the mutual coupling between the slots, which benefits impedance matching. In order to the low SLL characteristic, the radiation slots are rotated 45°. All the dimensions are also given in Fig. 1(b). The ridge GW in M4 feeds the sub-array through magnetic coupling. This causes unbalanced phase and amplitude at the output ports of the 1-to-4 cavity power divider in M3, if the hollow-waveguide is used as the coupling structure. Fig. 3(a) shows the simulated amplitude and phase responses of the cavity power divider. Excessive amplitude and phase imbalances appear at the output ports of the cavity power divider. One effective way to mitigate these imbalances is to use double-ridge waveguide instead of hollow waveguide for magnetic coupling. The improved amplitude and phase responses, within ± 0.5 dB and ± 1.5° respectively, are plotted in Fig. 3(b).

In the previous work [8], the basic array element of 45°-tilted 2×2 radiation slots is directly fed by the 1-to-4 cavity power divider (cavity in M3). Unfortunately, due to structural asymmetry, the amplitude and phase distributions among the four rotated radiation slots are imbalance, leading to grating lobes. [8] analyzed this in detail and provided a solution. This work presents an alternative solution. By using 1-to-2 cavity power dividers with symmetrical output ports in M2, the output signals can be restored to equal amplitude and in-phase responses. Fig. 4 shows the simulated S-parameters of the combined 1-to-8 vertical power divider in M3 and M2. Low amplitude variation of ± 0.07 dB and phase imbalance of ± 1.5° are achieved over the wide frequency range of 23 - 30 GHz.

Commonly, the cross polarization patterns deteriorate in a 45° linearly polarization array antenna. This is because the EM fields cannot be confined along E- and H-planes due to the

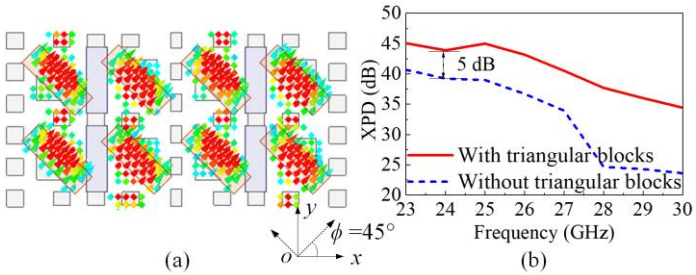

Fig. 5. (a) Simulated vector E-field in backed cavities in M2. (b) Comparison of XPD with and without triangular blocks.

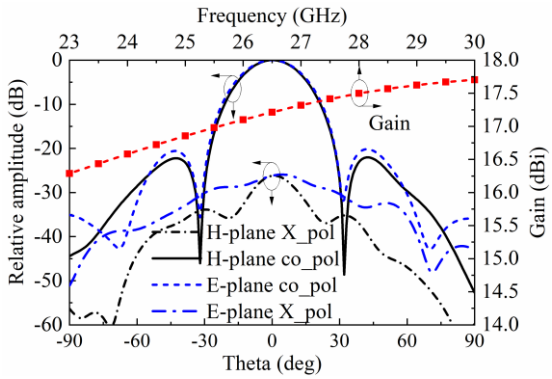

Fig. 6. Simulated radiation performances of the sub-array.

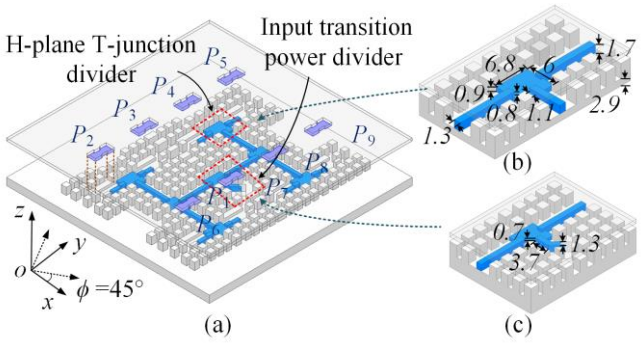

Fig. 7. Feed network. (a) 3-D view; (b) Basic H-plane T-junction; (c) Transition structure. All dimensions are given in millimeters.

inclined orientation of the radiation slots. To overcome this deficiency, two triangular blocks are added at the corners of each cavity in M2 to restrict the EM fields, as shown in Fig. 1(b). Fig. 5(a) shows the vector E-field distribution in the cavities. It is clear that the E-field is confined along the intended E-plane direction. The simulated XPDs of the sub-array with and without the triangular blocks are compared in Fig. 5(b). An improvement of over 5 dB to at least 34 dB XPD was achieved.

Fig. 6 illustrates the sub-array radiation performance. Note that the radiation patterns at the center frequency of 26.5 GHz is plotted in the intended E- and H-planes. The SLL is suppressed to under -20.5 dB. Over the desired frequency range, the peak gain is higher than 16.7 dBi.

C. Feed Network

A 1-to-8 (2×4) full corporate feed network in M4 is used to support the 8×8 radiation slots. Fig. 7(a) shows the whole feed network. It consists of multiple ridge GW H-plane T-junctions. Each T-junction is composed of a guiding ridge and a periodic pin surface in parallel-plate waveguide configuration. This is

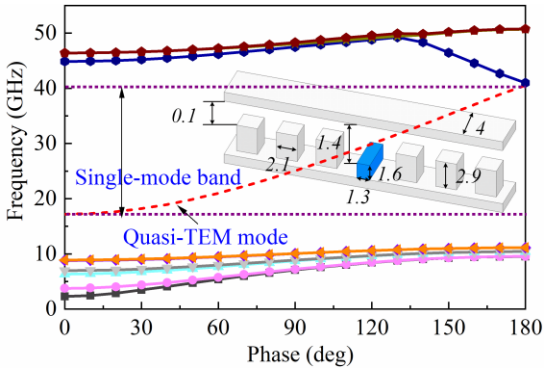

Fig. 8. Dispersion diagram for the ridge GW. All dimensions are given in millimeters.

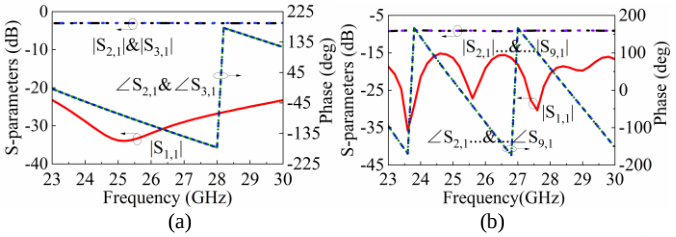

Fig. 9. Simulated S-parameters. (a) Basic H-plane T-junction; (b) Whole feed network.

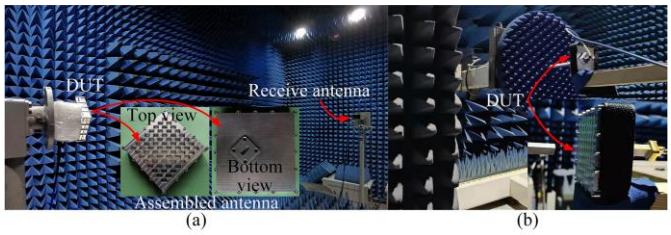

Fig. 10. Test environments. (a) Far-field system; (b) Near-field system.

shown in Fig. 7(b). The EM wave propagates between the ridge and the upper plate in quasi-TEM mode. The dispersion diagram of the pin unit cell is illustrated in Fig. 8. Only a single propagating mode (quasi-TEM mode) exists over 17–40 GHz, which covers the desired operating frequency band.

The simulated S-parameters of the basic H-plane T-junction are shown in Fig. 9(a). The reflection coefficient is lower than -20 dB with balanced amplitude and phase outputs over a wide frequency band of 23–30 GHz. To facility the measurement, standard WR-42 input waveguide is rotated 45° so that it is parallel with the radiation slots. A stepped guiding ridge structure is utilized to achieve the transition from WR-42 waveguide to ridge GW, as shown in Fig. 7(c). Fig. 9(b) shows the simulated S-parameters of the whole feed network. The reflection coefficient is less than -15 dB over the entire operating band. All the transmission coefficients are in-phase and the amplitudes are within -9±0.05 dB in the same band.

IV. Experimental Results

Four metallic blocks (radiation slot layer M1, cavity power divider layers M2 and M3, feed-network layer M4) are fabricated by milling on aluminum-magnesium alloy with a nominal conductivity of 3.1×10^7 S/m. Screws around the antenna is used to assemble the prototype. The photographs of fabricated blocks and assembled prototype are shown in Fig. 10. The overall size of the array antenna is 84 mm × 84 mm × 19.5

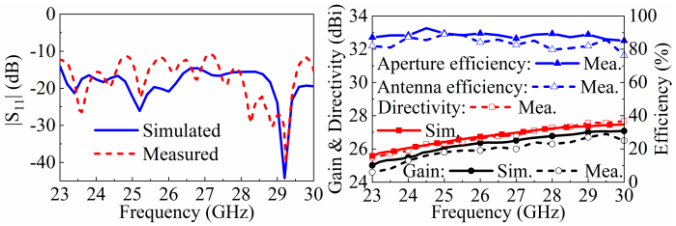

Fig. 11. Simulated and measured results. (a) $|S_{11}|$; (b) peak gain, directivity and antenna efficiency.

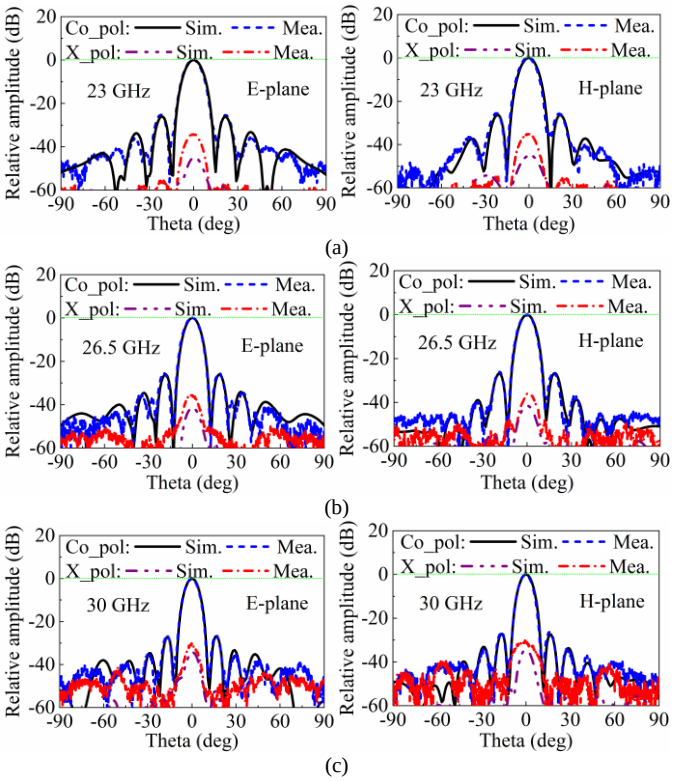

Fig. 12. Simulated and measured radiation patterns in the intended E-plane and H-plane at: (a) 23 GHz; (b) 26.5 GHz; (c) 30 GHz.

mm. The radiation performances are measured by a far-field test system in a microwave chamber, and the directivity and peak gain are obtained by a near-field test system.

A. Reflection Coefficient, Peak Gain, Directivity and Efficiency

Agilent E8361C network analyzer is used to measure reflection coefficient. Fig. 11(a) compares the measured and simulated results. A reasonable agreement is achieved. The FBW of $|S_{11}|$<-10.5 dB is 26.4% (from 23 to 30 GHz).

Fig. 11(b) plots the simulated and measured peak gain, directivity and antenna efficiency. Within the frequency band of 23 - 30 GHz, the measured peak gain varies from 24.6 – 26.9 dBi, which is about 0.19 -0.47 dBi lower than the simulation. The simulated and measured directivity varies from 25.6 – 27.4 dBi and 25.5 – 27.6 dBi, respectively. The small differences are mainly attributed to the fabrication tolerance and measurement error. The measured antenna efficiency and aperture efficiency based on the measured gain and directivity are also shown in Fig. 11(b). The antenna efficiency varies from 76.3% to 81.9% across the same frequency band, while the aperture efficiency is better than 85 %.

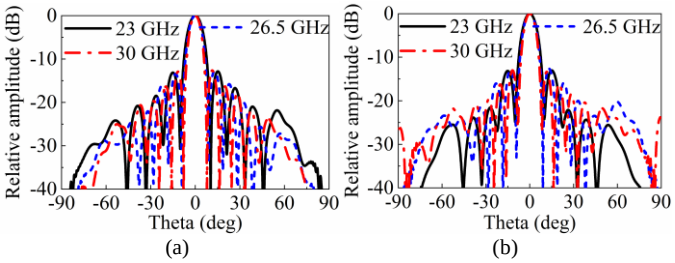

Fig. 13. Measured normalized radiation patterns. (a) Principal E-plane; (b) Principal H-plane.

TABLE I
COMPARISON OF WAVEGUIDE ANTENNA ARRAYS

Ref.	Antenna type	*f* (GHz) /BW (%)	SLL (dB)	Eff. (%)	Gain (dBi)	XPD (dB)
[8]	HW*+16×16 slots	61.5/9.6	-25.5	>70	32	>31.5
[9]	HW+16×16 slots	78.5/20.4	-26.2	>70	31.4	>30
[10]	HW+16×16 slots	78.5/25	-25.5	>74#	37.9	>32
[20]	GW+16×16 slots	60/17.6	-15	>60	--	>30
This work	GW+8×8 slots	26.5/26.4	-25.8	>76.3	24.6	>30.2

*HW: hollow waveguide.
#It is aperture efficiency in Ref. 10.

B. Radiation Patterns

The simulated and measured normalized radiation patterns in the intended E- and H-planes at three different frequencies are plotted in Fig. 12. The measured results are in good agreement with the simulated. The 3-dB beamwidths in the intended E- and H-planes are both larger than 7.2° over the entire frequency band. The measured SLLs are less than -25.8 dB. Fig. 12 also shows the measured cross polarization patterns. XPD are more than 30.2 dB for both planes within the operating band. Fig. 13 shows the measured radiation patterns in the principal E- and H-planes. The SLLs are around -13 dB, which are consistent to the radiation patterns with uniform excitation.

Table I compares this design with some previous published work. This work and [20] are based on GW technology, whereas others used hollow waveguide. In [20], good SLL and XPD were obtained without any optimization, due to the small tilting angle (10°) of the radiation slot. This work maintains excellent XPD and SLL even when the radiation gap rotates at a larger angle. Compared to other 45° polarized array antennas, this work achieved the widest frequency bandwidth and comparable radiation performances in terms of antenna efficiency, SLL, and peak gain.

V. CONCLUSION

In this letter, we have proposed a GW-based full corporate-fed 8×8-slot array antenna operating from 23 to 30 GHz. The additional layer of 1-to-2 cavity power dividers and triangular blocks loaded cavities are used to balance the amplitude and phase responses (avoiding the grating lobes) and improve XPD in a wide frequency band. A prototype is designed, fabricated and measured. Experimental results show that the antenna has high gain, low SLL, good XPD and antenna efficiency. With these features, the demonstrated antenna could find useful applications in 5G mmW front ends.

REFERENCES

[1] J. Xu, W. Hong, Z. H. Jiang, H. Zhang and K. Wu, "Low profile wideband vertically folded slotted circular patch array for Ka-band applications," *IEEE Trans. Antennas Propag.*, vol. 68, no. 9, pp. 6844-6849, Sep. 2020.

[2] Z. Talepour and A. Khaleghi, "Groove gap cavity slot array antenna for millimeter wave applications," *IEEE Trans. Antennas Propag.*, vol. 67, no. 1, pp. 659-664, Jan. 2019.

[3] D. Oueslati and R. Mittra, "Wideband fixed- and scanned-beam millimeter wave antenna arrays for 5G applications," in *14th European Conference on Antennas and Propagation (EuCAP)*, Copenhagen, Denmark, 2020, pp. 1-5.

[4] C. Mao, M. Khalily, P. Xiao, T. W. C. Brown and S. Gao, "Planar sub-millimeter-wave array antenna with enhanced gain and reduced sidelobes for 5G broadcast applications," *IEEE Trans. Antennas Propag.*, vol. 67, no. 1, pp. 160-168, Jan. 2019.

[5] P. Kumar, A. Kedar and A. K. Singh, "Design and development of low-cost low sidelobe level slotted waveguide antenna array in X-band," *IEEE Trans. Antennas Propag.*, vol. 63, no. 11, pp. 4723-4731, Nov. 2015.

[6] G. Huang, S. Zhou, T. Chio, H. Hui and T. Yeo, "A low profile and low sidelobe wideband slot antenna array fed by an amplitude-tapering waveguide feed-network," *IEEE Trans. Antennas Propag.*, vol. 63, no. 1, pp. 419-423, Jan. 2015.

[7] Y. J. Cheng, J. Wang and X. L. Liu, "94 GHz substrate integrated waveguide dual-circular-polarization shared-aperture parallel-plate long-slot array antenna with low sidelobe level," *IEEE Trans. Antennas Propag.*, vol. 65, no. 11, pp. 5855-5861, Nov. 2017.

[8] T. Tomura, Y. Miura, M. Zhang, J. Hirokawa and M. Ando, "A 45° linearly polarized hollow-waveguide corporate-feed slot array antenna in the 60-GHz band," *IEEE Trans. Antennas Propag.*, vol. 60, no. 8, pp. 3640-3646, Aug. 2012.

[9] T. Tomura, J. Hirokawa, T. Hirano and M. Ando, "A 45° linearly polarized hollow-waveguide 16×16-slot array antenna covering 71–86 GHz band," *IEEE Trans. Antennas Propag.*, vol. 62, no. 10, pp. 5061-5067, Oct. 2014.

[10] Y. You et al., "High-performance E-band continuous transverse stub array antenna with a 45° linear polarizer," *IEEE Antennas Wireless Propag. Lett.*, vol. 18, no. 10, pp. 2189-2193, Oct. 2019.

[11] L. Chang, Y. Li, Z. Zhang, X. Li, S. Wang and Z. Feng, "Low-sidelobe air-filled slot array fabricated using silicon micromachining technology for millimeter-wave application," *IEEE Trans. Antennas Propag.*, vol. 65, no. 8, pp. 4067-4074, Aug. 2017.

[12] P. Liu, J. Liu, W. Hu and X. Chen, "Hollow waveguide 32 × 32-slot array antenna covering 71–86 GHz band by the technology of a polyetherimide fabrication," *IEEE Antennas Wireless Propag. Lett.*, vol. 17, no. 9, pp. 1635-1638, Sep. 2018.

[13] P.-S. Kildal, "Artificially soft and hard surfaces in electromagnetics," *IEEE Trans. Antennas Propag.*, vol. 38, no. 10, pp. 1537–1544, Oct. 1990.

[14] P.-S. Kildal and M. N. M. Kehn, "The ridge gap waveguide as a wideband rectangular hard waveguide," in *Proc. 4th Eur. Conf. IEEE Antennas Propag. (EuCAP)*, Apr. 2010, pp. 1–4.

[15] P.-S. Kildal, E. Alfonso, A. Valero-Nogueira, and E. Rajo-Iglesias, "Local metamaterial-based waveguides in gaps between parallel metal plates," *IEEE Antennas Wireless Propag. Lett.*, vol. 8, no. 4, pp. 84–87, Apr. 2009.

[16] E. Pucci, E. Rajo-Iglesias, and P.-S. Kildal, "New microstrip gap waveguide on mushroom-type EBG for packaging of microwave components," *IEEE Microw. Wireless Compon. Lett.*, vol. 22, no. 3, pp. 129-131, Mar. 2012.

[17] A. Vosoogh and P.-S. Kildal, "Corporate-fed planar 60 GHz slot array made of three unconnected metal layers using AMC pin surface for the Gap waveguide," *IEEE Antennas Wireless Propag. Lett.*, vol. 15, pp. 1935-1938, 2016.

[18] H. S. Farahani and W. Bösch, "Ku-band gap waveguide filter with negative coupling structure," in *European Microwave Conference in Central Europe (EuMCE)*, Prague, Czech Republic, 2019, pp. 290-293.

[19] M. Rezaee, A. U. Zaman, and P.-S. Kildal, "V-band groove gap waveguide diplexer," in *Proc. IEEE 9th Eur. Conf. Antennas Propag. (EuCAP)*, May 2015, pp. 1–4.

[20] A. Vosoogh, P. Kildal and V. Vassilev, "Wideband and high-gain corporate-fed gap waveguide slot array antenna with ETSI class II radiation pattern in V-Band," *IEEE Trans. Antennas Propag.*, vol. 65, no. 4, pp. 1823-1831, April 2017.